International Journal of Heat and Mass Transfer 80 (2015) 227–235

Contents lists available at ScienceDirect

International Journal of Heat and Mass Transfer

journal homepage: www.elsevier.com/locate/ijhmt

Characteristics analysis and parametric study of a thermoelectric generator by considering variable material properties and heat losses

Jing-Hui Meng [a], Xin-Xin Zhang [a], Xiao-Dong Wang [b,c,*]

[a] School of Mechanical Engineering, University of Science and Technology Beijing, Beijing 100083, China
[b] State Key Laboratory of Alternate Electrical Power System with Renewable Energy Sources, North China Electric Power University, Beijing 102206, China
[c] Beijing Key Laboratory of Multiphase Flow and Heat Transfer for Low Grade Energy, North China Electric Power University, Beijing 102206, China

ARTICLE INFO

Article history:
Received 30 November 2013
Received in revised form 23 July 2014
Accepted 11 September 2014
Available online 29 September 2014

Keywords:
Thermoelectric generator
Variable properties
Heat losses
Optimization
Output power
Conversion efficiency

ABSTRACT

The output power and conversion efficiency of the thermoelectric generator (TEG) are closely related to not only the materials properties but also the geometric structure. This paper developed a multi-physics, steady-state, and three-dimensional numerical TEG model to investigate the TEG performance, and then the model is compared with the classical thermal resistance model. Bismuth-telluride are used as p- and n-type materials. The comparison reveals that the assumption of constant material properties leads to underestimated inner electrical resistance, and overestimated thermal conductance and Seebeck coefficient, so that the thermal resistance model predicts unrealistically high performance than the present model. The results also indicate that when heat losses exist between the TEG and the ambient, although the output power is slightly elevated, the conversion efficiency is significantly reduced, hence, improvement of the heat insulation effect is critically important for high-temperature TEGs. Furthermore, the TEG geometry also affects its performance significantly: usage of thin ceramic plates increases the junction temperature difference, and hence enhances the TEG performance; there are two optimal leg lengths which correspond to the maximum output power and the maximum conversion efficiency, respectively; when heat losses are not ignorable, a large semiconductor cross-sectional area remarkably reduces the ratio of the heat liberated to the ambient to the heat absorbed from the high-temperature heat source, and hence improves the conversion efficiency.

1. Introduction

Energy conservation and emissions reduction issue has become a global consensus due to the serious greenhouse effect and climate change. Hence, renewable energy sources, such as wind, solar, hydro and geothermal energy, have made a considerable development and progress in the last decades. As one of such alternatives, thermoelectric generator (TEG) directly converts heat into electricity by Seebeck effect of thermoelectric materials. The TEG is more robust, flexible and reliable when compared with convectional power generators, because it requires neither real working fluids nor moving parts, so that it is attracting more and more attention [1–12].

The output power and conversion efficiency as indicators for evaluating the TEG performance are closely related to the figure-of-merit of thermoelectric materials, $ZT = \alpha^2\sigma T/\lambda$, where α is the Seebeck coefficient, σ is the electric conductivity, λ is the thermal conductivity, and T is the absolute temperature at which the properties are measured [13–15]. Thermoelectric materials with larger ZT can improve the TEG performance. Previous research has demonstrated that α, σ, and λ for most thermoelectric materials are all strongly temperature-dependent. It should be noted that the TEG generally works at a higher temperature difference than the thermoelectric cooler (TEC), such as the recycling of waste heat for iron and steel industry. Thus, it is expected that the temperature-dependent materials properties have much significant effect on the TEG performance. In the previous research, the thermal resistance model was widely used to investigate the TEG performance, and the model is still most frequently adopted so far. This kind of model can derive analytical expressions of the output power and conversion efficiency, so that it can be applied for preliminary screening of TEG design and performance estimation. However, the model accounts for energy balances only at the hot end and the cold end of the TEG. As a result, the constant [1–4,6,8,10–12], or temperature-averaged [5] materials properties

* Corresponding author at: State Key Laboratory of Alternate Electrical Power System with Renewable Energy Sources, North China Electric Power University, Beijing 102206, China. Tel./fax: +86 10 62321277.
E-mail address: wangxd99@gmail.com (X.-D. Wang).

http://dx.doi.org/10.1016/j.ijheatmasstransfer.2014.09.023
0017-9310/

must be assumed. Recently, Chen et al. [9] proposed and implemented a 3D numerical model for TEG in FLUENT UDS (User Defined Scalar) environment. Using the same model, Reddy et al. [16] investigated the performance of a novel composite thermoelectric device where a major part of the semiconductor is replaced with a conductor such as copper. In their studies [9,16], the great influence of materials properties are emphasized on the TEG performance. We also developed general, steady-state or transient, 3D numerical models of thermoelectric devices [17–19], in which the heat conduction equation and the electric potential equation were solved coupled and all thermoelectric effects were taken into account, including Seebeck effect, Peltier effect, Thomson effect, Joule heating, Fourier's heat conduction, and heat loss to the ambient. The materials properties were proven to have significant effect not only on the steady-state performance but also on dynamic characteristics for TEC. However, there is no detailed explanations in the literature how materials properties affect the TEG performance.

In addition to the materials properties (α, σ, λ, or ZT), the geometric structure of the TEG also significantly affects its performance. By optimizing the ceramic plate thickness, the leg length and the cross-sectional area of semiconductors, a high-performance TEG can be designed. Some research has already studied the geometric-dependent TEG performance using the thermal resistance model [20–22], or one-dimensional model [23,24]. However, the three-dimensional temperature effect cannot be ignored when there exist significant heat losses from the TEG to the ambient. Recently, Jang et al. [25] investigated the optimal structure of high-performance micro-TEG at room temperature using a three-dimensional model. However, constant materials properties are adopted in their work, because the TEG operates with only a 15 K temperature difference.

This work develops a multi-physics, steady-state, and three-dimensional numerical TEG model to investigate the optimal TEG geometric structure. The proposed model is compared with the classical thermal resistance model to demonstrate the effects of temperature-dependent materials properties and heat losses on the accurate prediction of the TEG performance. Especially, this paper will explain from the heat transfer mechanism why the thermal resistance model predicts unrealistically high performance of TEG. The article structure arrangement is organized as follows. Sections 2 and 3 describe and validate the new three-dimensional TEG model. Section 4 compares the new model with the conventional thermal resistance model to highlight the effect of temperature-dependent materials properties. Section 5 reveals the reduction in the TEG performance due to its heat losses to the ambient. Finally, the optimal structure parameters of the TEG are discussed in Section 6, including the ceramic plate thickness (Section 6.1), the leg length (Section 6.2), and the cross-sectional area (Section 6.3) of semiconductors.

2. Model

2.1. Numerical model

As the basic element of a practical TEG, the p–n junction is formed by connecting two different types of thermoelectric materials (the hole-rich p-type semiconductor and the electron-rich n-type semiconductor) together. When a temperature difference is supplied to the two sides of the junction, the thermal excitation causes migration of carriers from the hot side to the cold side, so that a Thomson electromotive force will be created. In addition, there exists a concentration difference of carriers between p- and n-type materials, which activates the electrons diffusion from the n-type material to the p-type material and the back diffusion of holes. As a result, a Peltier electromotive force will be constructed. The Seebeck electromotive force is the sum of the Thomson and Peltier electromotive forces, which is a maximum electric potential produced by the junction and is also referred as to the open-circuit voltage. However, when a load is connected to the junction, the junction cannot produce the electric potential difference as large as the open-circuit voltage because of the electric potential drop caused by inner electrical resistance of the junction. To obtain a higher output voltage, many p–n junctions need to be connected in series to form a TEG.

Fig. 1 shows the schematic of a TEG unit, where a p–n junction (n-doped and p-doped bismuth-telluride legs) is connected electrically in series by copper connectors, and is sandwiched between two same ceramic plates (silicon). As electrical insulation layer, the ceramic plate plays a role in thermal conduction from outer heat sources and cooling parts to p–n junction.

The three-dimensional, steady-state TEG model developed here solves heat and electricity conductions simultaneously. The governing equations and boundary conditions are as follows.

2.1.1. Heat conduction equations

$$\nabla \cdot (\lambda_i \nabla \mathrm{T}) + \frac{J^2}{\sigma_i} - \beta_i \vec{J} \cdot \nabla T = 0 \tag{1}$$

where λ is the thermal conductivity, σ is the electric conductivity, and β is the Thomson coefficient. The subscript i denotes conn for the connectors, p for the p-type semiconductor, n for the n-type semiconductor, cer for the ceramic plates, respectively. $\vec{J}$ is the local current density vector and equals zero for the ceramic plates. The first term on the left side in Eq. (1) denotes the Fourier heat conduction, and the second and third terms denote the Joule heating and Thomson effect, respectively.

2.1.2. Electric potential equation

$$\nabla \cdot (\sigma(\nabla \phi - \alpha \nabla T)) = 0 \tag{2}$$

where α is the Seebeck coefficient of semiconductors, ϕ is the electric potential, $\alpha \nabla T$ is Seebeck electromotive force coming from the Seebeck effect.

The Thomson coefficient is proportional to the first derivative of the Seebeck coefficient versus temperature, or:

$$\beta = T \frac{\mathrm{d}\alpha}{\mathrm{d}T} \tag{3}$$

Once the electric potential is obtained, the current density vector can be calculated by the following equation:

$$\vec{J} = \sigma \vec{E} = \sigma(-\nabla \phi + \alpha \nabla T) \tag{4}$$

2.1.3. Boundary conditions

The boundary conditions are described in Fig. 1. The temperatures at the top of the upper ceramic plate and the bottom of the lower ceramic plate are 450 K and 300 K, respectively. At the interfaces between different materials, temperature and heat flux are all assumed continuous. The side surfaces of n- and p-type semiconductors are convective boundary conditions, or:

$$-\lambda \frac{\partial T}{\partial n} = h(T - T_\infty) \tag{5}$$

where h is the convective heat transfer coefficient, T_∞ is the ambient temperature assumed to be 300 K. The boundary conditions for electric conduction include: (1) at the side surface of the connector under the n-type semiconductor: $J = I/A_c$ = constant, where I is the load current and A_c is the side surface area of the

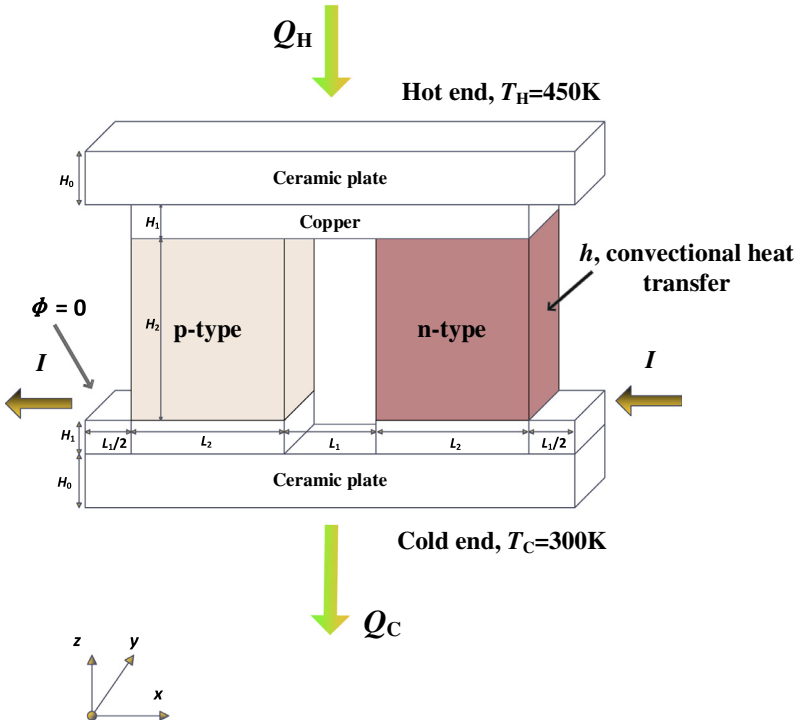

Fig. 1. Schematic of TEG unit.

connector; (2) at the side surface of the connector under the p-type semiconductor: $\phi = 0$.

2.1.4. The TEG performance

Generally, the performance of the TEG is evaluated by two parameters, the output power P and conversion efficiency η, which are defined as follows, respectively:

$$P = IV \tag{6}$$

$$\eta = \frac{P}{Q_H} \tag{7}$$

where V is the output voltage, Q_H is the heat supplied to the hot end of the TEG.

2.2. Solution procedure

The solution procedure for the present coupled model is described briefly in the following: (1) make the initial guess for temperature and electric potential; (2) create geometry and grids of the TEG model; (3) specify all boundary conditions; (4) solve the electric potential by Eq. (2); (5) calculate the local current density vector by Eq. (4); (6) solve the temperature by Eq. (1); (7) calculate the Seebeck coefficient, Thomson coefficient, electric conductivity, and thermal conductivity of all materials by the correlations in Table 1; (8) and then return to step (4) until the convergent iterative solutions are achieved.

2.3. Thermal resistance model

One of the objectives of this work is to compare the new three-dimensional TEG model with the conventional thermal resistance model, and hence the thermal resistance model is also introduced briefly here. Restated that the thermal resistance model does not solve the distributions of temperature and electric potential within the TEG, and it considers heat balances only at the hot and cold ends of the TEG. Consequently, the total electrical resistance R, Seebeck coefficient A and thermal conductance K for the p–n junction must be defined, or:

$$R = \frac{H_p}{\sigma_p S_p} + \frac{H_n}{\sigma_n S_n} \tag{8}$$

$$A = \alpha_p - \alpha_n \tag{9}$$

$$K = \frac{\lambda_p S_p}{H_p} + \frac{\lambda_n S_n}{H_n} \tag{10}$$

where $H_p = H_n = H_2$, $S_p = S_n = L_2 \times L_2$.

The heat balance equations for the hot and cold ends can be respectively expressed as:

Table 1
Material properties used in the present simulations.

Parameters	Semiconductor		Connector (Cu)	Ceramic plate (Si)
	Constant property	Variable property		
k (W K^{-1} m^{-1})	$k_p = k_n$ 1.54	$k_p = k_n$ $0.000029T^2 - 0.019593T + 4.809677$	350	130
ρ (Ω m)	$\rho_p = \rho_n$ 1.03×10^{-5}	$\rho_p = \rho_n$ $10^{-6}(0.043542T - 2.754139)$	1.695×10^{-9}	–
α (V K^{-1})	$\alpha_p = -\alpha_n$ 2.0×10^{-5}	$\alpha_p = -\alpha_n$ $10^{-6}(-0.002025T^2 + 1.423448T - 44.953611)$	6.5×10^{-6}	–
Source	[26]	[26]	[25]	[25]

$$Q_H = (T_H - T_{H,j})D_H \tag{11}$$

$$Q_H = AIT_{H,j} - \frac{1}{2}I^2R + K(T_{H,j} - T_{C,j}) \tag{12}$$

$$Q_C = AIT_{C,j} + \frac{1}{2}I^2R + K(T_{H,j} - T_{C,j}) \tag{13}$$

$$Q_C = (T_{C,j} - T_C)D_C \tag{14}$$

$$P = Q_H - Q_C = AI(T_{H,j} - T_{C,j}) - I^2R \tag{15}$$

where Q_H, I, T_H, T_C and P have the same meaning as in the numerical model, Q_C is the heat flow rate liberated from the TEG unit to the heat sink, $T_{H,j}$ and $T_{C,j}$ are the temperatures of the hot and cold junctions, D_H and D_C are the thermal conductances of the upper and lower ceramic plates. The heat flows $AIT_{H,j}$ and $AIT_{C,j}$ caused by the Peltier effect are released from the hot junction and absorbed at the cold junction, respectively. Joule heating I^2R due to the flow of electrical current through the p–n junction is generated inside the p–n junction. It should be noted that the Joule heating in the thermal resistance model is generally assumed to be equally distributed to the hot and cold junctions. The heat flow $(T_H - T_{H,j})D_H$ through the ceramic plate at the hot end, $(T_{C,j} - T_C)D_H$ through the ceramic plate at the cold end, and $K(T_{H,j} - T_{C,j})$ through the p–n junction are caused by the Fourier heat conductions.

3. Model validation

The same bismuth-telluride materials with temperature-dependent properties are adopted as the p-type and n-type semiconductors. The silicon and copper are respectively selected as the ceramic plate and connector, their properties are assumed to be constant due to ignorable thermoelectric effect. The properties for all the materials can be found in Table 1.

The grid sensitivity analysis is performed for the present TEG model to check its grid independence, where four grid systems are designated as grid (i), grid (ii), grid (iii) and grid (iv), respectively. The geometric parameters of the TEG unit and corresponding grid number are listed in Table 2. The temperature difference between the hot and cold ends is assumed to be $\Delta T = T_H - T_C = 150$ K with the convective heat transfer coefficient $h = 0$ W m^{-2} K^{-1}. Fig. 2 shows P and η of the TEG unit as functions of I for the four grid schemes. At $I < 0.1$ A, there are almost no differences in P and η predicted by the four grid schemes, while $I > 0.1$ A, the differences for P and η occur, and become more obvious as the current growing. The maximum deviation between grids (ii) and (iii) is 1.07%, it reduced to 0.64% for grids (iii) and (iv). Grid (iii) was chosen for the simulations as a tradeoff between accuracy and execution time.

The present TEG model is compared with one-dimensional steady-state analytical solution of Angrist et al. [27] and numerical model of Chen et al. [9]. The geometry and material properties used here are the same with Angrist et al.'s solution and Chen et al.'s simulation. The TEG device includes 127 units, each unit has the geometry of $H_1 = 0.2$ mm, $H_2 = 1.6$ mm, $L_1 = 0.5$ mm, and $L_2 = 1.4$ mm, as well as constant material properties of $\alpha_p = -\alpha_n = 226.8 \times 10^{-6}$ V K^{-1}, $k_p = k_n = 1.52$ W m^{-1} K^{-1} and $\sigma_p = \sigma_n = 1.447 \times 10^{-5}$ Ω m. The TEG operates at $T_H = 423$ K and

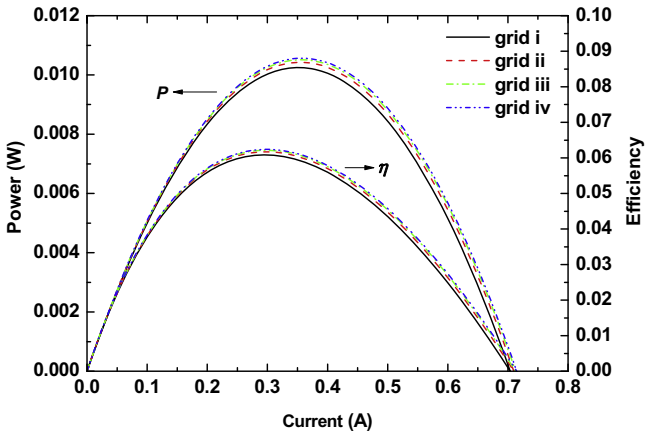

Fig. 2. Grid independence examination.

Table 3
Comparisons of numerical and analytical results ($T_H = 423$ K and $T_C = 303$ K).

Quantity	Present results	Analytical results [27]	Chen et al.'s results [9]
Q_H (W)	81.2	81.3	81.8
P (W)	3.88	3.98	3.62
I (A)	1.08	1.08	1.032
n	4.77	4.89	4.43

$T_C = 303$ K, and the heat losses to the ambient are ignored. With these conditions, Q_H, P, I, and η are predicted by the three models. Table 3 shows that the present prediction has better agreement with the analytical solution than Chen et al.'s. It should be pointed that the analytical solution [27] is strictly true only when the TEG has one-dimensional temperature distribution, uniform current density, constant material properties, and no heat losses to the ambient. However, the present model is more general with three-dimensional distributions of temperature and current density, which can be used to study the TEG performance at more complicated operating conditions such as high temperature difference and/or large heat losses to the ambient.

4. Comparison between three-dimensional model and thermal resistance model

As stated above, the thermal resistance model is the most frequently adopted in literature, and the model can only use constant materials properties because the inner temperature distribution of the TEG is not solved. To improve the accuracy, the reference temperature for materials properties is generally taken as $T_{ref} = (T_H + T_C)/2$. However, the present model uses temperature-dependent properties, thus, comparison between the two models can highlight the effect of temperature-dependent materials properties. The comparison is performed at $\Delta T = 30$ K, 60 K, 90 K, 120 K or 150 K with a fixed $T_C = 300$ K.

Table 2
The geometric parameters and test grid numbers for TEG.

Geometry	Value	L_1	L_2	L_3	H_1	H_2	H_3
		0.1 mm	0.5 mm	0.2 mm	0.2 mm	0.1 mm	1.0 mm
Grid (i)	Grid number	2	10	4	4	2	20
Grid (ii)	Grid number	3	15	6	6	3	30
Grid (iii)	Grid number	4	20	8	8	4	40
Grid (iv)	Grid number	5	25	10	10	5	50

Fig. 3 shows the I–P curves for both the models at different ΔT. The I–P curves are all typical parabola for the two models, P firstly increases and then drops as the current increases, hence there exists a maximum output power, P_{max}. P_{max} is elevated when ΔT is increased. In addition, both the models predict that as ΔT is increased, the effective working currents, defined as the current when $P \geqslant 0$, are all increased, for example, at $\Delta T = 30$ K, the effective working current interval for the present model is $0 < I < 0.13$ A, and increases to $0 < I < 0.23$ A when $\Delta T = 60$ K.

Fig. 3 also indicates that although the variation trend of P as the function of I and ΔT predicted by the thermal resistance model is similar with the present model, the quantitative differences between the two models are significant, especially for high I and large ΔT. The differences include that the thermal resistance model overestimates P and the maximum effective working current. The overestimation can be explained as follows. Because the present model has solved distributions of the temperature and electrical potential, the open-circuit voltage (V_o) and the output voltage can be directly obtained. Thus, the effective electrical resistance can be calculated as $R = (V_o - V)/I$, which is shown in Fig. 4. It can be seen that R in the thermal resistance model remains constant according to Eq. (8), however, R in the present model is higher than that in the thermal resistance model, and their difference becomes larger as I increases. Consequently, the overestimation of P in the thermal resistance model can be attributed to the underestimation of R according to Eq. (15). In addition, with $P = 0$, Eq. (15) can be rearranged as follows:

$$I_{max} = \frac{A(T_{H,j} - T_{C,j})}{R} \tag{16}$$

where I_{max} is the maximum working current. Based on the same reason, I_{max} in the thermal resistance model is also overestimated.

Fig. 5 shows the heat absorbed at the hot end of the TEG unit for the two models at various ΔT. Compared with the present model, the thermal resistance model predicts a larger Q_H, especially for large I. According to Eq. (12), Q_H can be split into three parts: the Peltier heat, Joule heat and Fourier heat conduction, their contributions for $\Delta T = 150$ K are presented in Fig. 6. Due to the quadratic relationship between the Joule heat and I, the Joule heat calculated by the two models has only a small difference. As a plain heat source, Peltier heat is generated only on the interface between two semiconductors or two conductors. The reference temperature for $\alpha(T)$ in the Peltier heat ($=\alpha(T)IT$) should be taken as the interface temperature. Thus, we have $\alpha = \alpha(T_{H,j})$ for the hot junction. However, when the approach with temperature-averaged properties are adopted, almost all of thermal resistance models assume $\alpha = \alpha(T_{ref})$ [22,28–31]. For bismuth-telluride materials, α has a negative temperature effect, $\alpha(T_{ref})$ is larger than $\alpha(T_{H,j})$ due to

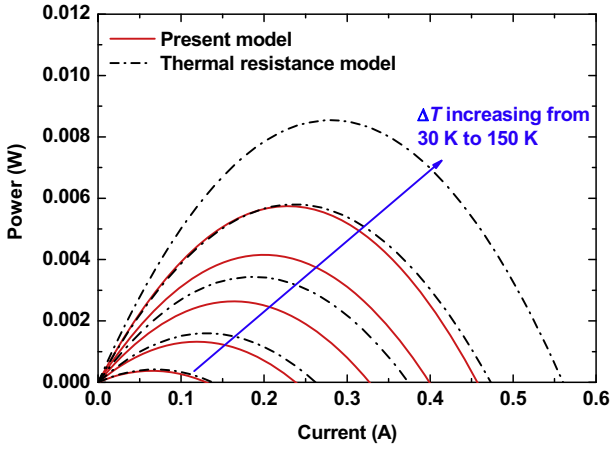

Fig. 3. The output power of the TEG unit for constant and variable properties at various temperature differences.

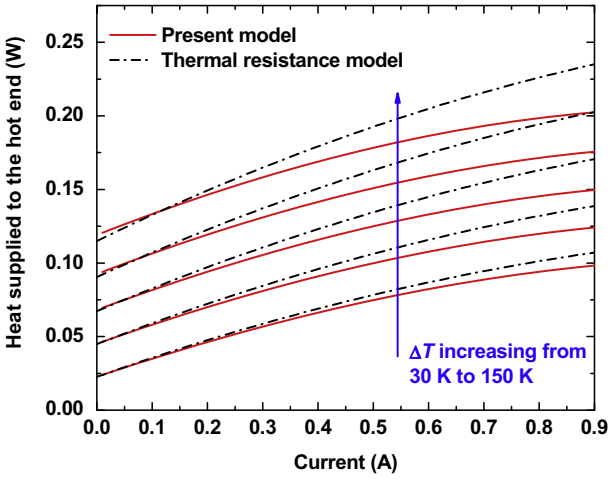

Fig. 5. The heat absorbed at the hot end of the TEG unit for constant and variable properties at various temperature differences.

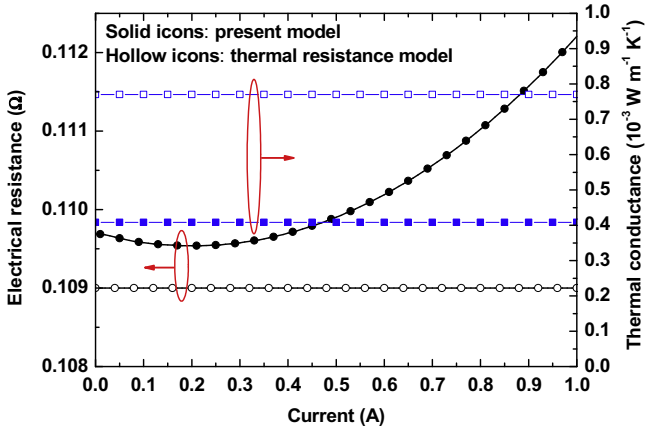

Fig. 4. Variations of the total electrical resistance and the total thermal conductance with I at $\Delta T = 150$ K.

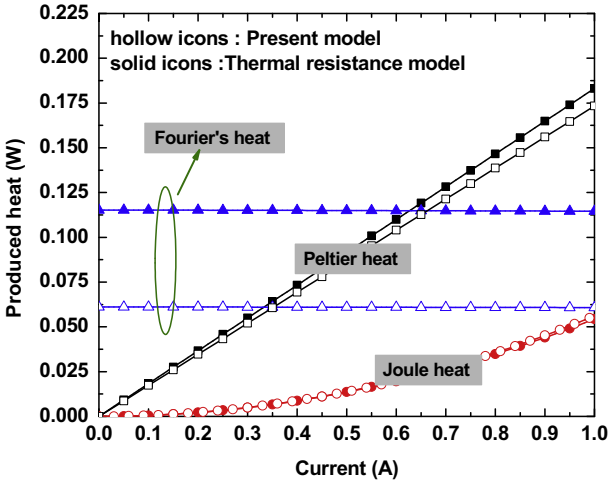

Fig. 6. The produced heat within the TEG unit for $\Delta T = 150$ K.

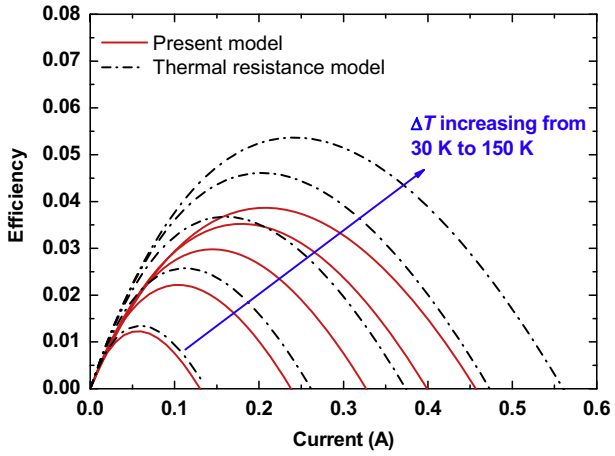

Fig. 7. The conversion efficiency of the TEG unit for constant and variable properties at various temperature differences.

$T_{ref} < T_{H,j}$. Therefore, the thermal resistance model overestimates the Peltier heat on the hot junction, as shown in Fig. 6. According to Eq. (10), the total thermal conductance of the p–n junction is 7.70×10^{-4} W K^{-1} for the thermal resistance model. However, this thermal conductance is actually related to ΔT and the functional relation between λ and T of p- and n-type semiconductors, which can be calculated by solving only the heat conduction equation (Eq. (1)) for the same TEG geometry and the same ΔT, while all thermoelectric effects are ignored. With $\Delta T = 150$ K, the thermal conductance for the p–n junction is found to be only 4.08×10^{-4} W K^{-1} (Fig. 4). Thus, the thermal resistance model overestimates the contribution of Fourier heat conduction. As a result, the thermal resistance model predicts a larger Q_H.

Fig. 7 shows η of the TEG unit as a function of I at various ΔT for the two models. Comparison of Figs. 3 and 5 indicates that although P and Q_H are all overestimated by the thermal resistance model, the overestimation of P is more significant. Hence, η is also overestimated significantly by the thermal resistance model. For example, the maximum conversion efficiencies, η_{max}, are 3.85% and 5.38% for the two models at $\Delta T = 150$ K, respectively, and the thermal resistance model overestimates η_{max} by 39.74%.

5. Effect of heat losses

In practical applications, the TEG has the promising potential for the recycling of industrial waste heat such as in iron and steel industry, where the waste heat temperature is generally higher than 450 K [32], so that the performance of the TEG is inevitably affected by heat losses between the TEG and the ambient. It should be noted that the thermal resistance model cannot take heat losses into account, hence, the effects of heat losses are investigated only by the present model with temperature-dependent properties at $\Delta T = 150$ K. The value of total heat transfer coefficient (h) is assumed to be 0–200 W m^{-2} K^{-1}[17], which combines contributions of the convection and radiation.

Fig. 8 shows variations of P and η for various h at $\Delta T = 150$ K. At $I < 0.12$ A, h has a ignorable effect on P, while at $I > 0.12$ A, its effect is elevated gradually as I increases. The occurrence of heat losses reduces the inner temperature of the TEG, and the reduction is found to be more significant for high h (Fig. 9). For bismuth-telluride materials, the electrical resistivity has a positive temperature effect, as a result of the reduced inner temperature, the effective electrical resistance and inner electric potential drop of the p–n junction are both reduced when h is increased. On the other hand, the open-circuit voltage remains almost unchanged for various h.

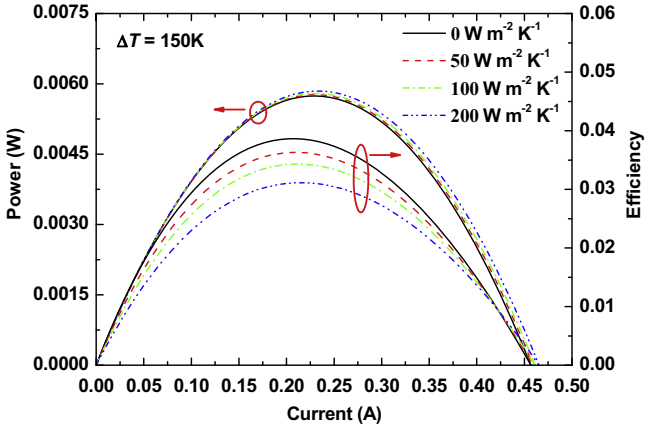

Fig. 8. Performance of the TEG unit with various h at $\Delta T = 150$ K.

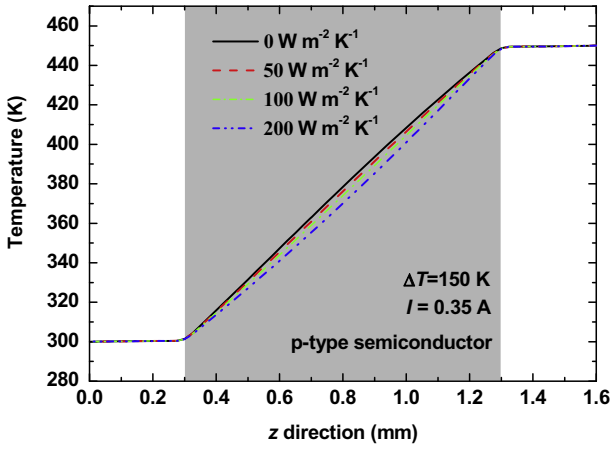

Fig. 9. Temperature distribution of z direction along the center of p-type semiconductor with various h at $\Delta T = 150$ K.

Hence, the higher output voltage ($V = V_o - IR$) and output power ($P = IV$) occur at a larger h. For the same reason in Section 4, the effective working current interval increases as h is increased. At $h = 0$ W m^{-2} K^{-1}, the maximum effective working current is 0.45 A, it increases to 0.46 A when $h = 200$ W m^{-2} K^{-1}.

Although the heat losses slightly elevate the output power, the conversion efficiency is significantly reduced as h increases. A higher h means that more heat will be transferred to the ambient

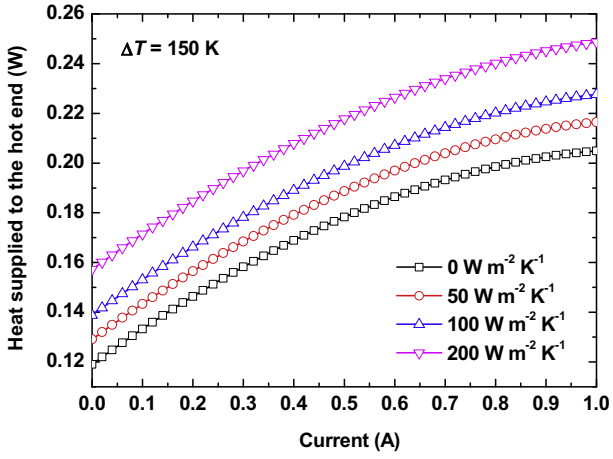

Fig. 10. Absorbed heat at the hot end of the TEG unit for various h at $\Delta T = 150$ K.

from the TEG, hence, a larger Q_H will be needed to keep the constant $\Delta T = 150$ K (Fig. 10). The result indicates that the high output power comes at the cost of conversion efficiency, thus, the heat losses should be reduced as small as possible when a TEG operates. For example, as shown in Fig. 10, P_{max} is 5.74×10^{-3} W for $h = 0$ W m^{-2} K^{-1} and 5.85×10^{-3} W for $h = 200$ W m^{-2} K^{-1}, which is increased by only 1.92%, however, η_{max} is decreased by 19.43% (=(3.86% − 3.11%)/3.86%).

6. Parametric study of TEG geometry

Effect of the TEG geometry on the performance is investigated by the present model and the thermal resistance model. Because the performance predicted by the two models has almost no qualitative differences but quantitative differences, and Section 4 has already explained why the thermal resistance model overestimates the performance of the TEG unit, thus, this section will just demonstrate their difference but not repeat the explanation. The output power and conversion efficiency for the TEG with various geometries are compared at three characteristic currents (small, intermediate, and large) for Sections 6.1 and 6.2 or two current densities for Section 6.3. The temperature difference is chosen as $\Delta T = 150$ K with $h = 100$ W m^{-2} K^{-1} for the present model and $h = 0$ W m^{-2} K^{-1} for the thermal resistance model.

6.1. Effect of ceramic plate thickness

As the electrical insulator, the ceramic plate transfers heat from the outside heat source to the p–n junction as well as from the p–n junction to the outside heat sink. Due to non-zero thermal resistance of the ceramic plate, its thickness directly affects the temperatures of hot and cold junctions, and hence has significant impact on the TEG performance, as shown in Fig. 11. At the three characteristic currents of 0.1, 0.2, and 0.4 A, P and η decrease linearly as the ceramic plate thickness increases, this is mainly because the temperature difference ($T_{H,j} - T_{C,j}$) between the hot and cold junctions becomes smaller as the plate gets thicker, which reduces the Seebeck electromotive force, and hence reduces the open-circuit voltage. Fig. 11 confirms again the difference in the performance predicted by two models, and the difference becomes more significant at high I, therefore, the thermal resistance model is only applicable for preliminary scanning of TEG performance.

6.2. Effect of semiconductor leg length

Effect of semiconductor leg length on the performance of the TEG unit is shown in Fig. 12. As the leg length increases, P and η first reach their peak values (P_{max} and η_{max}) at a certain length, then monotonically drop. It is worth noting that for the three characteristic currents, the optimal leg length corresponding to P_{max} is almost the same, however, the leg length corresponding to η_{max} is different from each other, which moves toward longer length direction at low current. Thus, to design high-performance TEGs, one has to make a choice between the two optimal leg lengths.

Fig. 12(a) also shows that P_{max} is elevated as I increases, but the maximum leg length is reduced. For example, the maximum length predicted by the present model is larger than 5.00 mm at $I = 0.1$ A,

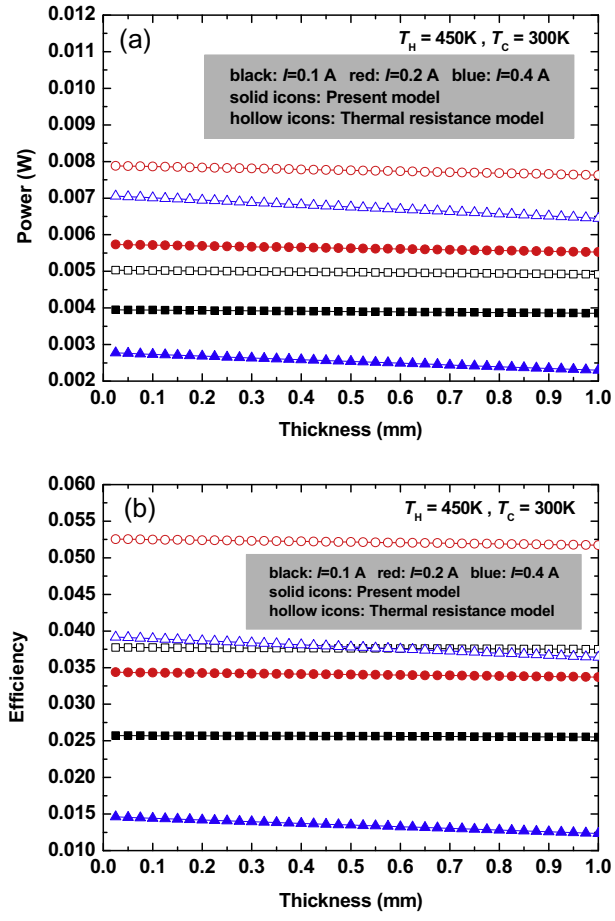

Fig. 11. TEG performance for various ceramic plate thicknesses at different currents: (a) output power; (b) conversion efficiency.

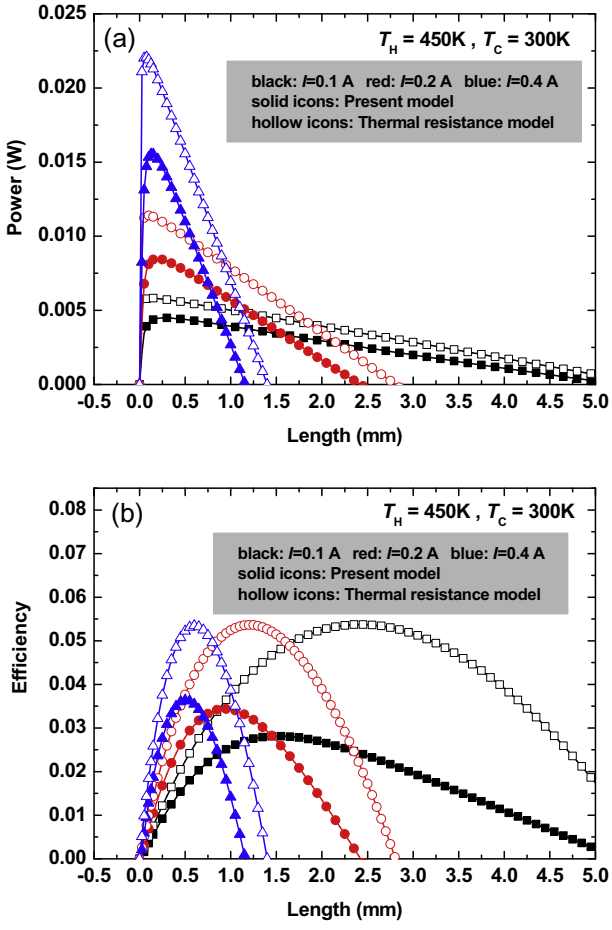

Fig. 12. TEG performance for various leg lengths at different currents: (a) output power; (b) conversion efficiency.

however, the maximum length is reduced to 2.40 mm at $I = 0.2$ A and 1.15 mm at $I = 0.4$ A. This can be explained using the following relation:

$$R_{max} = \frac{A(T_{H,j} - T_{C,j})}{I} \tag{17}$$

With the fixed ceramic plate thickness and semiconductor materials, the open-circuit voltage, $A(T_{H,j} - T_{C,j})$, are almost the same for different leg lengths and currents. According to Eq. (17), the maximum of the total electrical resistance of the p–n junction should be less for a higher I, thus, the maximum leg length becomes small.

6.3. Effect of cross-sectional area of semiconductor

Effect of cross-sectional area of semiconductors ($S_p = S_n$) on the TEG performance is investigated at $T_H = 450$ K and $T_C = 300$ K. For fair comparison, the same current density (J) for various S_p and the output power per unit cross-sectional area ($P_{area} = P/S_p$) are used here.

Fig. 13 confirms again that the thermal resistance model overestimates the TEG performance. Fig. 13(a) shows that P_{area} almost remains unchanged at various S_p for the thermal resistance model, however, the present model predicts that the TEG has better performance at a small S_p. According to the thermal resistance model, P_{area} meets:

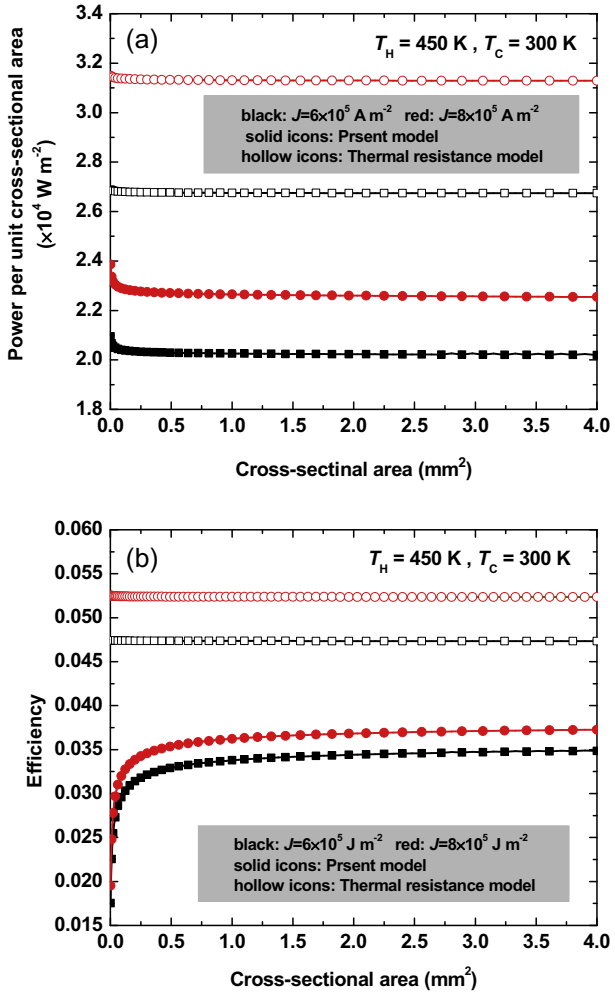

Fig. 13. TEG performance for various cross-sectional areas at different current densities: (a) output power per unit cross-sectional area; (b) conversion efficiency.

$$P_{area} = \frac{Q_H - Q_C}{S_p} = AJ(T_{H,j} - T_{c,j}) - \left(\frac{H_p}{\sigma_p} + \frac{H_n}{\sigma_n}\right)J^2 \tag{18}$$

Eq. (18) indicates that P_{area} is independent on S_p. However, because the present model solves the temperature field, the difference of the temperature distribution within semiconductors for various S_p causes their inner electrical resistance changes, and the p–n junction with a smaller S_p has a lower inner electrical resistance, so that a larger P_{area} occurs at the smaller S_p.

Fig. 13b shows the variation of η with S_p. According to Eq. (12), the absorbed heat per unit cross-sectional area ($Q_{area} = Q_H/S_p$) is also independent on S_p, thus, $\eta = P_{area}/Q_{area}$ remains almost unchanged due to the same energy input and output for the thermal resistance model. However, for the present model, η increases first rapidly then slowly with the increased S_p. Restated that the present model takes heat losses (Q_{loss}) into account, although the TEG with a large S_p has a large total convective heat transfer area ($S_{conv,total}$), the ratio of convective heat transfer area to semiconductor cross-sectional area ($S_{conv,total}/S_p$) reduces, which implies that the heat losses per unit semiconductor cross-sectional area ($Q_{loss,area} = Q_{loss}/S_p$) becomes smaller for the large S_p. For example, $Q_{loss,area} = 117683$ W m^{-2} for $J = 8 \times 10^5$ A m^{-2} and $L_2 \times L_2 = 0.25$ mm^2, which reduces to 59845 W m^{-2} for $J = 8 \times 10^5$ A m^{-2} and $L_2 \times L_2 = 1$ mm^2. Consequently, to maintain a fixed temperature difference 150 K, more heat needs to be input into the hot end for the TEG with small S_p, so that η reduces as S_p decreases. The results above indicate that for a practical TEG operation, when the heat losses are not ignorable, a large S_p should be recommended.

7. Conclusions

This paper develops a three-dimensional and steady-state TEG model, which couples the temperature and electric potential equations and accounted for all thermoelectric effects, including the Seebeck effect, Peltier effect, Thomson effect, Joule heating and Fourier's heat conduction. The model is used to investigate effects of the temperature-dependent material properties, heat losses, and TEG geometry on the TEG performance. The main conclusions are as follows:

(1) The present model is compared with the classical thermal resistance model in a wide range of currents and temperature differences. The comparison shows that the thermal resistance model overestimates the output power and conversion efficiency of the TEG, it is especially true at large currents and high temperature differences. The overestimated performance can be attributed to the fact that the thermal resistance model does not solve the temperature distributions within the TEG and can only adopt the assumption of the constant or temperature-averaged material properties. For bismuth-telluride materials used in this work, the electrical resistivity has a positive temperature effect and the Seebeck coefficient has a negative temperature effect. Thermal resistance model with temperature-averaged properties predicts a much lower effective inner electrical resistance of the p–n junction, and the much higher Peltier heat on the hot junction and Fourier heat conduction, consequently, overestimates the TEG performance.

(2) Although the heat losses slightly elevate the output power, the conversion efficiency is significantly reduced as the total heat transfer coefficient increases. With higher total heat transfer coefficient, the hot end of the TEG should absorb more heat to maintain a fixed temperature difference, which leads to a remarkable reduction in conversion efficiency. Therefore, for a real TEG operation, the heat losses should be reduced as small as possible.

(3) The TEG geometric parameters have significant effect on its performance. As the ceramic plate becomes thicker, the TEG performance deteriorates due to the reduced temperature difference between the hot and cold junctions. For a specific TEG, there are two optimal leg lengths of semiconductors corresponding to the maximum output power and maximum conversion efficiency, respectively. When the heat losses are not ignorable, a large cross-sectional area should be recommended.

Conflict of interest

None declared.

Acknowledgments

This study was partially supported by the National Nature Science Foundation of China (No. 51276060), by the National Key Basic Research Program of China (No. 2012CB720401), and by the 111 Project (No. B13004).

References

[1] S. Kim, Analysis and modeling of effective temperature differences and electrical parameters of thermoelectric generators, Appl. Energy 102 (2013) 1458–1463.
[2] S. Kumar, S.D. Heister, X. Xu, J.R. Salvador, G.P. Meisenr, Thermoelectric generators for automotive waste heat recovery systems. Part I: Numerical modeling and baseline model analysis, J. Electron. Mater. 42 (2013) 665–674.
[3] Y.Y. Hsiao, W.C. Chang, S.L. Chen, A mathematic model of thermoelectric module with applications on waste heat recovery from automobile engine, Energy 35 (2010) 1447–1454.
[4] M. Eswaramoorthy, S. Shanmugam, A numerical model to compute heat loss in the focal receiver of a solar parabolic dish thermoelectric generator, Energy Sources Part A – Recov. Utilizat. Environ. Effects 34 (2012) 959–965.
[5] X. Gao, S.J. Andreasen, M. Chen, S.K. Kær, Numerical model of a thermoelectric generator with compact plate-fin heat exchanger for high temperature PEM fuel cell exhaust heat recovery, Int. J. Hydrogen Energy 37 (2012) 8490–8498.
[6] K. McEnaney, D. Kraemer, Z. Ren, G. Chen, Modeling of concentrating solar thermoelectric generators, J. Appl. Phys. 110 (2011) 074502.
[7] D.T. Crane, An introduction to system-level, steady-state and transient modeling and optimization of high-power-density thermoelectric generator devices made of segmented thermoelectric elements, J. Electron. Mater. 40 (2011) 561–569.
[8] G.W. Liang, J.M. Zhou, X.Z. Huang, Analytical model of parallel thermoelectric generator, Appl. Energy 88 (2011) 5193–5199.
[9] M. Chen, L.A. Rosendahl, T. Condra, A three-dimensional numerical model of thermoelectric generators in fluid power systems, Int. J. Heat Mass Transfer 54 (2011) 345–355.
[10] H. Xiao, X.L. Gou, S.W. Yang, Detailed modeling and irreversible transfer process analysis of a multi-element thermoelectric generator system, J. Electron. Mater. 40 (2011) 1195–1201.
[11] F. Meng, L. Chen, F. Sun, A numerical model and comparative investigation of a thermoelectric generator with multi-irreversibilities, Energy 36 (2011) 3513–3522.
[12] N. Espinosa, M. Lazard, L. Aixala, H. Scherrer, Modeling a thermoelectric generator applied to diesel automotive heat recovery, J. Electron. Mater. 39 (2010) 1446–1455.
[13] D.M. Rowe, Thermoelectrics Handbook: Macro to Nano, CRC Press, Boca Raton, 2006.
[14] S.B. Riffat, X. Ma, Thermoelectrics: a review of present and potential applications, Appl. Therm. Eng. 23 (2003) 913–935.
[15] F.J. Disalvo, Thermoelectric cooling and power generation, Science 285 (1999) 703–706.
[16] B.V.K. Reddy, M. Barry, J. Li, M.K. Chyu, Mathematical modeling and numerical characterization of composite thermoelectric devices, Int. J. Therm. Sci. 67 (2013) 53–63.
[17] X.D. Wang, Y.X. Huang, C.H. Cheng, D.T.W. Lin, A three-dimensional numerical modeling of thermoelectric device with consideration of coupling of temperature field and electric potential field, Energy 47 (2012) 488–497.
[18] J.H. Meng, X.D. Wang, X.X. Zhang, Transient modeling and dynamic characteristics of thermoelectric cooler, Appl. Energy 108 (2013) 340–348.
[19] J.H. Meng, X.X. Zhang, X.D. Wang, Dynamic response characteristics of thermoelectric generator predicted by a three-dimensional heat-electricity coupled model, J. Power Sources 245 (2014) 262–269.
[20] D. Kraemer, K. McEnaney, M. Chiesa, G. Chen, Modeling and optimization of solar thermoelectric generators for terrestrial applications, Sol. Energy 86 (2012) 1338–1350.
[21] J. Chen, B. Lin, H. Wang, G. Lin, Optimal design of a multi-couple thermoelectric generator, Semicond. Sci. Tech. 15 (2000) 184–188.
[22] B.S. Yilbas, A.Z. Sahin, Thermoelectric device and optimum external load parameter and slenderness ratio, Energy 35 (2010) 5380–5384.
[23] D.M. Rowe, M. Gao, Evaluation of thermoelectric modules for power generation, J. Power Sources 73 (1998) 193–198.
[24] D.L.W. Silva, M. Kaviany, Micro-thermoelectric cooler: interfacial effects on thermal and electrical transport, Int. J. Heat. Mass Transfer 47 (2004) 2417–2435.
[25] B. Jang, S. Han, J.Y. Kim, Optimal design for micro-thermoelectric generators using finite element analysis, Microelectron. Eng. 88 (2011) 775–778.
[26] A. Martinez, D. Astrain, A. Rodriguez, Dynamic model for simulation of thermoelectric self-cooling applications, Energy 55 (2013) 1114–1126.
[27] S.W. Angrist, Direct Energy Conversion, third ed., Allyn and Bacon, 1976.
[28] A.S. Al-Merbati, B.S. Yilbas, A.Z. Sahin, Thermodynamics and thermal stress analysis of thermoelectric power generator: influence of pin geometry on device performance, Appl. Therm. Eng. 50 (2013) 683–692.
[29] M. Yamanashi, A new approach to optimum design in thermoelectric cooling systems, J. Appl. Phys. 80 (1996) 5494–5502.
[30] Y.H. Cheng, C. Shih, Maximizing the cooling capacity and COP of two-stage thermoelectric coolers through genetic algorithm, Appl. Therm. Eng. 26 (2006) 937–947.
[31] X.C. Xuan, K.C. Ng, C. Yap, H.T. Chua, The maximum temperature difference and polar characteristic of two-stage thermoelectric coolers, Cryogenics 42 (2002) 273–278.
[32] M.E. Ertem, S. Gürgen, Energy balance analysis for Erdemir blast furnace number one, Appl. Therm. Eng. 26 (2006) 1139–1148.